IEEE Access
Multidisciplinary | Rapid Review | Open Access Journal

Received March 19, 2019, accepted April 4, 2019, date of publication April 11, 2019, date of current version April 25, 2019.

Digital Object Identifier 10.1109/ACCESS.2019.2910659

A Study on IR Target Recognition Approach in Aerial Jamming Environment Based on Bayesian Probabilistic Model

SHAOYI LI[1], KAI ZHANG[1], JIANFEI YIN[2], AND KAI YANG[1]
[1]School of Aeronautics, Northwestern Polytechnical University, Xi'an, China
[2]Shanghai Aerospace Control Technology Institute, Shanghai, China

Corresponding author: Shaoyi Li (amlishaoyi2008@163.com)

This work was supported in part by the National Natural Science Foundation of China under Grant 61703337, and in part by the Shanghai Academy of Spaceflight Technology Innovation Foundation under Grant SAST2017-082.

ABSTRACT The use of infrared (IR) decoys as a countermeasure has become a significant and important factor that influences the performance of heat-seeking missiles. The system employed by such missiles utilizes a template matching algorithm that relies on the infrared characteristics of the target. This target feature vector is compared against the features of nearby objects using minimum distance classification criterion. One of the problems is that it is very difficult to efficiently consider every possible jamming condition. This paper confronts the issue using Bayesian methods to build a probabilistic recognition model that performs well in an aerial jamming environment. Our approach is based on simulating the partial reasoning functions of human visual cognition, where the Bayesian component is used to handle uncertainty. Dealing with ambiguity, such as distinguishing between target and decoy, requires a properly trained model. Our solution, in part, is to conduct a feature histogram analysis on a large set of data that are generated by using a simulated method. This produces a feature probability model with a mixed Gaussian distribution. The maximum likelihood estimation is performed to determine the class of the object, and as such distinguish between genuine targets and decoys. We extend this to construct a new aerial IR target recognition algorithm that relies on both prior information and our probabilistic recognition model. Our empirical analysis includes simulated aerial combat images that are generated for the purpose of testing our method. The experimental results indicate that our approach shows an improvement in performance when compared to the feature template matching approach.

INDEX TERMS Feature histogram, feature probability distribution function, mixed Gaussian distribution, naive Bayesian classifier, target recognition.

I. INTRODUCTION

Currently, most of imaging missiles use IR imaging guidance because of better anti-jamming ability and the working capability in day and night. IR target recognition algorithms in the complex environment are very important for attacking the airplane targets. It directly results in the performance of IR seeker and the accuracy of hitting the targets. A missile attack on military targets is both real and current threat. As a result, there is a great deal of interest in developing countermeasures to prevent this from happening. In this paper we discuss the IR thermal imaging homing missile, and the contribution that our research of the IR recognition algorithms can make towards thwarting certain countermeasures. Techniques used to confuse thermal imaging systems include the use of IR decoys and laser jamming [1], [2]. These, among others, have become an effective means to protect various targets against this type of threat. Accordingly, the study of IR target recognition algorithms in the heat seeker is of intense interest to researchers working in the field of missile anti-jamming [3], [4].

The working phase of the infrared thermal imaging seeker includes target acquisition and target tracking phase. Generally, the target acquisition phase mainly realizes detecting weak and small targets in a complex background. At this stage, the target gray, contrast and trajectory characteristics

The associate editor coordinating the review of this manuscript and approving it for publication was Bora Onat.

(a) (b)

FIGURE 1. The aerial jamming environment.

are used to complete the target detection. The target tracking phase mainly achieves target recognition and stable tracking in the jamming environment after the target is located and identified. At this stage, the seeker measures the error deviating from the image center and drives the servo stabilization platform in order to hold the optical axis to always point to the target. That is, the target is always in the center of the image under ideal condition. But it is impossible to directly extract the real trajectory features of the target. Usually, the target recognition is realized by using gray, shape, and statistical features within the single frame. In this paper, the target recognition problem in the jamming environment occurs in the target tracking phase, which is different from the target tracking problem in the general video surveillance system [5], [6]. As shown in Fig. 1, launching an IR decoy in the vicinity of the target will cause feature confusion, resulting in obfuscation of the target. This severely detracts from the effectiveness of IR target recognition and missile's ability to recognize. Therefore, for the missile to perform successfully, it is crucial that the IR target recognition system is able to properly identify its target. This identification includes the ability to distinguish the genuine target and any possible decoys or imaginary images.

Currently, a typical IR target recognition algorithm uses the target's infrared characteristics to assist with automatic target recognition [7]–[9]. The IR characteristics are based on the target's image template and the similarity measurement criterion. For the purpose of developing a model, the image feature template is treated as prior knowledge. The problem with systems of this type rests in the difference between theory and practice, where the true environment is both complex and dynamic. In practice, it is difficult to acquire realistic and sufficient information about potential targets. This jamming image template, as well as other data used by the missile's anti-jamming process, can appear dissimilar depending on environmental factors. There is a cognitive limitation with respect to how much information the missile can gather or deduce about the target, and furthermore, it is hard to cover all of the test conditions. These issues imply that IR target recognition algorithm adapts poorly to new and unknown environments. This is problematic, and it would seem that target recognition of the IR thermal imaging system is facing considerable plight.

Inspired by the application of the Bayesian approach for both text classification and image target detection [10]–[12], the main contribution of this research involves building a novel IR target recognition algorithm based on a probabilistic model. Our work also involves partially replicating the functionality of human visual cognition, and training the model using a large number of data samples generated by way of simulation. This model will process the information available on the target and decoy images with the goal of discerning them. Ultimately, the model is used to develop a new algorithm with enhanced accuracy in aerial IR target recognition, while many testing works have been done in order to analyzing the anti-jamming performance under various launching conditions of IR decoys.

This paper's contents are arranged as follows: the second section reviews traditional aerial IR target recognition algorithms. Section three introduces the probabilistic recognition model, which incorporates the replication of human visual cognition and the Bayesian methods. The fourth section constructs a new aerial IR target recognition strategy that is based on the probabilistic recognition model. Section five explains the experimental approach and describes our experiments. This includes a presentation and analysis of our results. Finally, section sixth includes our summary, conclusion and plans for future work.

II. RELATED WORK

The task of target recognition in an aerial jamming environment relies on a similarity measurement criterion to rule out noise created by jamming efforts. It does so by examining various segments of the data that are similar to the target, and then applying a distance measure between each of them and the expected target profile. The task needs to work efficiently, and take into consideration the real-time processing requirements of an IR thermal imaging system. In this paper, several different states are considered and form the basis of the following definitions:

(a) Input feature vector: This is the input for the classifier.

(b) Target feature template: This is the target feature vector.

(c) Jamming feature template: This is the jamming feature vector.

To distinguish the target and jamming vectors, the system uses high-efficiency minimum distance as the classification criterion. It measures the distance between the input feature vector and each feature template to determine which has the minimum and maximum differences. Based on these calculations it makes a determination that which vector represents the target.

Assuming that m reference vectors $R_1, R_2, \ldots, R_m$ in m classes respectively belong to classes $\omega_1, \omega_2, \ldots, \omega_m$. In this paper m is equal to 2, while vectors R_1 and R_2 respectively represent feature templates belonging to the target class ω_1, and the jamming class ω_2. For the current feature vector X_i, which belongs to one of N candidate areas, the target and jamming vectors are evaluated according to the following criterion.

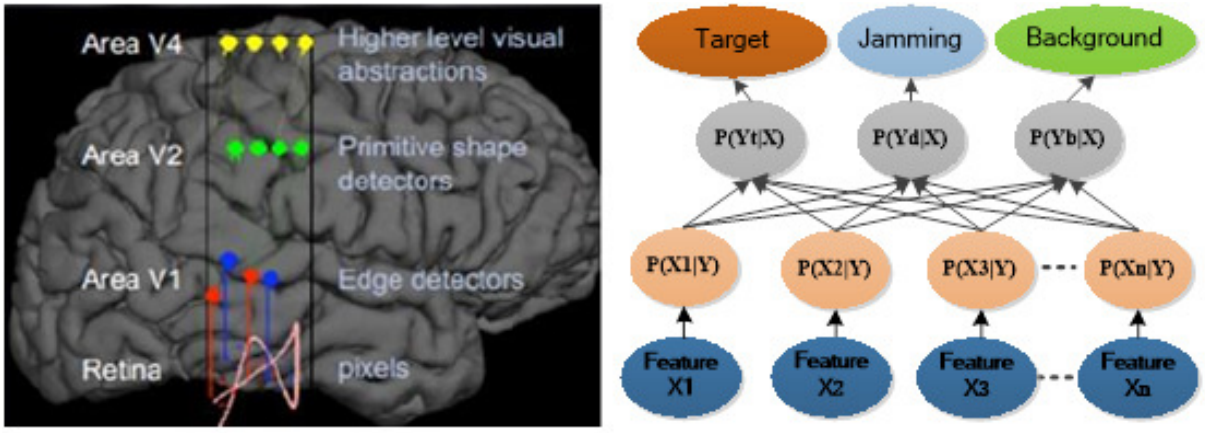

FIGURE 2. Simple probability framework based on human visual cognition.

First, k labeling areas I_k with the nearest distances between X_i and R_1 are found by:

$$I_k = \{i_1, \ldots, i_k | D(X_{i_j}, R_1) \leq T, i_j \in N, j = 1, \ldots, k\}, \quad (1)$$

where $D(X_l, R_1) = \sqrt{(X_l - R_1)^T (X_j - R_1)} (l \in N)$ and T is a constant determined by means of measurement during experiments. The target area label $\hat{i}_t$ with the maximal distance between $X_{\hat{i}_t}$ and R_2 is found by:

$$\hat{i}_t = \texttt{arg max}_{j \in I_k} D(X_j, R_2), \quad (2)$$

where $\hat{i}_t$ is the target area label and $X_{\hat{i}_t}$ is the feature vector corresponding to ω_1.

III. PROBABILISTIC RECOGNITION MODEL

A. PROBABILITY FRAMEWORK OF HUMAN VISUAL COGNITION

The human languages contain a large number of words related to the frequency or probability of an occurrence. Some words of this are 'possible', 'probable', 'seem', 'think','certain', 'definite', and 'sure'. This suggests that when objects in the physical world are processed by the visual system, they are classified according to a certain probability description [13]. This is done by refining key information (such as distinguishing features), applying judgment and decision-making (probability criterion) according to certain criteria, and then assigning probability based on the results. Consider the following three statements and the differences that they imply: "I thought I saw a cat", "I think it is a cat", and "I'm sure that is a cat." We assert that these are distinguished by the features that are available for consideration, and how these features are weighed. Perhaps there are partial features or key features that influence the probability, along with the total number of features available for analysis. Based on our own knowledge and memory, we determine whether these match the conditions of feature set $\mathbf{X} = \{X_1, X_2, X_3, \ldots, X_n\}$. Hence, we can infer the probability of a cat $P(Y|\mathbf{X})$.

Goodale and Lee have discovered that the human visual system is hierarchical. The levels range from the low-level edge features in V1, to the partial features of a shape or target in V2, up to the higher-level features in V4. The level of abstraction in the feature representation is correlated with the ambiguity of the target description, and also with the probability of making a correct judgement with respect to identification. Therefore, it is greatly beneficial to understand how various images are classified [14], [15]. With respect to the issue at hand, this paper proposes that in combination with the prior knowledge, this problem can be represented by a simple probability framework that simulates human visual cognition. The probability of target, decoy and jamming noise has the feature set $\mathbf{X}$ is $P(\mathbf{X}|\mathbf{Y_C})$, $\mathbf{Y_C} = \{Y_1, Y_2, Y_3\}$, where Y_1 represents the target, Y_2 the IR decoy and Y_3 the other jamming efforts. This framework satisfies the conditions that the feature vector $\mathbf{x} = (x_1, x_2, x_3, \ldots, x_n)$ and the conditional probability of target, decoy and background jamming is $P(Y_i|\mathbf{X} = \mathbf{x})$, $i = 1, 2, 3$. Each scenario is classified as the maximum posterior probability criterion. The principle is shown in Fig. 2.

B. PROBABILISTIC RECOGNITION MODEL WITH BAYESIAN APPROACH

This paper introduces a probability framework to solve the problem of aerial target recognition. The data for analysis may contain misleading features that are the result of an IR decoy or other noise related to jamming. The feature set used for describing the environment is comprised primarily of texture features, motion features and shape features. The texture feature includes descriptors such as maximum gray, mean gray, and energy. The motion feature includes related labels such as speed, trajectory change rate, etc. Finally, the shape feature describes length-width ratio, circumference, area, center of gravity, etc. A set of public feature variables are selected from the set to make up the feature vector $\mathbf{X} = (X_1, X_2, X_3, \ldots, X_n)$. The feature membership probability $P(Y_i|\mathbf{X} = \mathbf{x})$ can be adopted to describe the

probability of the target, IR decoy and background jamming when the feature vector $\mathbf{X}$ is a designated value. If the specified threshold condition is satisfied then the target is recognized, where $X_1, X_2, X_3, \ldots, X_n$ represent feature variables $\mathbf{x} = (x_1, x_2, x_3, \ldots, x_n)$, it follows that x_i represents the value of the feature variable X_i; $x_i \in \mathbf{\Omega}$, where $\mathbf{\Omega}$ is the valid range; Y_i represents the target class; i respectively represent the target, IR decoy and background jamming noise.

The probability framework in this paper is a type of graph that is based on Bayesian theory, also called a Bayesian classifier. The biggest challenge for the Bayesian classifier is to compute the joint probability $P(\mathbf{X}, Y_i)$; And the simplest method used to solve this issue is the naive Bayesian model [16]. If Y_i is given, then all of the variables X_i are conditionally independent:

$$\begin{aligned} P(\mathbf{X}, Y_i) &= P\{X_1, X_2, \ldots, X_n, Y_i\} \\ &= P(Y_i)P(X_1|Y_i)P(X_2|Y_i)\ldots P(X_n|Y_i) \end{aligned} \tag{3}$$

where $P(Y_i)$ is the prior probability of the target class, and $P(X_j|Y_i)$ is conditional probability of X_j given Y_i. In our model this class-conditional probability density is $i = 1, 2, 3$, $j = 1, 2, \ldots, n$. The Bayesian formula states that the classification can be converted into a given $\mathbf{X} = \mathbf{x}$ by computing the posterior probability $P(Y_i|\mathbf{X} = \mathbf{x})$, and solving the maximum posterior probability:

$$\begin{aligned} P(Y_i|\mathbf{X} = \mathbf{x}) &= \frac{P(\mathbf{X}, Y_i)}{\sum_{i=1}^{3} P(\mathbf{X}, Y_i)} \\ &= \frac{P(\mathbf{X}, Y_i)P(Y_i)}{\sum_{i=1}^{3} P(\mathbf{X} = \mathbf{x}, Y_i)P(Y_i)} \end{aligned} \tag{4}$$

The formula is further expanded as follows:

$$P(Y_i|\mathbf{X}=\mathbf{x}) = \frac{P(Y_i)P(X_1|Y_i)P(X_2|Y_i)\ldots P(X_n|Y_i)}{\sum_{i=1}^{3} P(Y_i)P(X_1|Y_i)P(X_2|Y_i)\ldots P(X_n|Y_i)} \tag{5}$$

For all of the classes, because the above-mentioned formula $\sum_{i=1}^{3} P(Y_i)P(X_1|Y_i)P(X_2|Y_i)\ldots P(X_n|Y_i)$ is constant, and assuming that the attribute values are mutually independent, according to maximum posterior criterion, the following formula is adopted to classify the feature vector $\mathbf{x}$:

$$\begin{aligned} \hat{Y} &= \texttt{arg max}_{\hat{Y} \in \mathbf{Y}_C} P(Y_i|\mathbf{X} = \mathbf{x}) \\ &= \texttt{arg max}_{\hat{Y} \in \mathbf{Y}_C} \{P(\mathbf{X} = \mathbf{x}|Y_i)P(Y_i)\} \end{aligned} \tag{6}$$

where the class prior parameter $\theta = P(Y_i)$ can be estimated via statistical analysis of the number of classes in the training set $\mathbf{D}$ based on the smoothing approach:

$$\hat{\theta} = \frac{N_C + \alpha}{N + C\alpha} \tag{7}$$

where N_C is the number of samples belonging to the Y_i class in the training set, N is the sum of the various classes in the sample data, $\alpha \geq 0$, and $\alpha = 1$ is Laplacian smoothing [13].

Nevertheless, in order to estimate $P(\mathbf{X} = \mathbf{x}|Y_i)$, it is necessary to assume a feature distribution or generate a non-parametric model for the solution.

C. FEATURE PROBABILITY DENSITY-FUNCTION MODEL

Deriving the feature distribution is a difficult problem via theoretical analysis. The feature distribution law can be recognized by employing a statistical approach. While, this is dependent on whether there are sufficient training samples and a reasonable assumption is made on that basis. In terms of the IR images being referenced, the gray histogram is a function related to the gray scale distribution. The algorithm determines the frequency of each gray value in the image mathematically. Then, this paper introduces the feature histogram approach [17] to describe the frequency of each class of feature value. For example, how often is one of the feature values mean gray in the training set.

For a training set $\mathbf{D}$ that includes N samples, and the range of each class of values is $[0, L_k - 1]$, $k = 0, 1, \ldots, n$, where n is number of the selected feature, the normalized histogram of any class of feature can be represented as follows:

$$P(r_k, t) = \frac{n_{k,t}}{N} \tag{8}$$

where r_k is t^{th} value of k^{th} feature; $r_{k,t} \in [0, L_k - 1]$, where $n_{k,t}$ is the total number of feature values $r_{k,t}$ in the training set.

With respect to the training samples that have a certain feature in common, the statistics are compiled and a histogram can be used to visualize the commonalities. This is done by setting the horizontal coordinate as the feature value, with its frequency set as the vertical coordinate. Such a histogram will reflect the probability distribution law of a given feature. Fig. 3 depicts the histogram of the mean gray value from four different perspectives. The first describes the target(refer Fig. 3(a)), while another more generally describes the area of the target(refer Fig. 3(c)). Similarly in the next two diagrams, we can see the mean gray of the IR decoy(refer Fig. 3(b)) compared to that of the IR decoy area(refer Fig. 3(d)). It is clear that the histograms are of both unimodal and multimodal types. A unimodal curve is relatively close to Gaussian distribution, while the multimodal differs significantly.

1) GAUSSIAN MODEL FOR FEATURE PROBABILITY DISTRIBUTION FUNCTION

Accordingly, the feature histograms curve can approximately be described by the Gaussian model (GM) [10]. Assuming that $(X_{k1}, X_{k2}, \ldots X_{kN})$ is an instance of X_k, its value is $(x_{k1}, x_{k2}, \ldots x_{kN})$, $\boldsymbol{\theta}_k = (\boldsymbol{\mu}_k, \boldsymbol{\sigma}_k)$. The maximum likelihood (ML) [17] is taken from the training dataset $\boldsymbol{D}$ to estimate $\boldsymbol{\theta}_k$. The likelihood function is represented as:

$$\begin{aligned} \mathtt{L}(\boldsymbol{\theta}_k) &= \prod_{i=1}^{N} \mathbf{N}(x_{k,i}|\boldsymbol{\omega}_k, \boldsymbol{\mu}_k, \boldsymbol{\sigma}_k^2) \\ &= \prod_{i=1}^{N} \frac{1}{\sqrt{2\pi}\sigma_k} \exp(-\frac{(x_{k,i} - \mu_k)^2}{2\sigma_k^2}) \end{aligned} \tag{9}$$

Furthermore, the parameter estimation of $\boldsymbol{\theta}_k$ is as follows:

$$\hat{\mu}_k = \frac{1}{N} \sum_{i=1}^{N} x_{k,i} \tag{10}$$

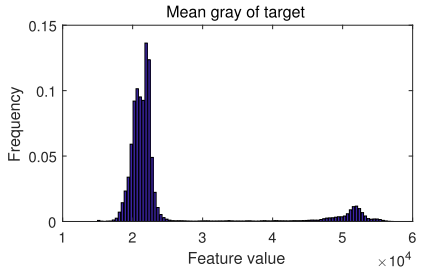

(a)

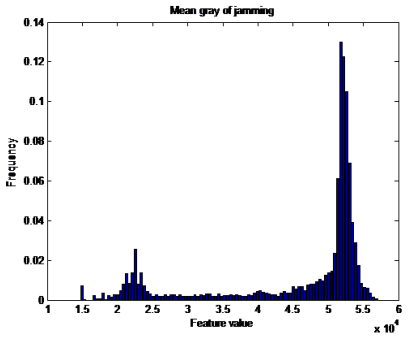

(b)

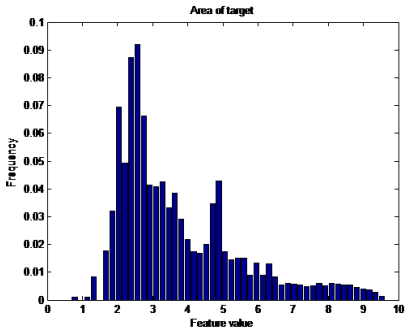

(c)

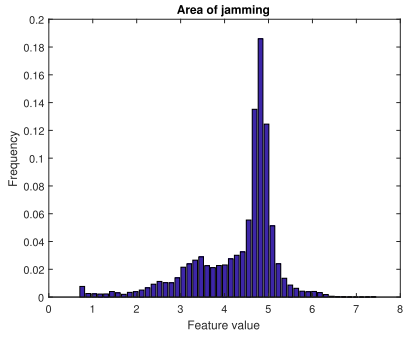

(d)

FIGURE 3. The feature histogram of (a) the mean gray attribute of target, (b) the mean gray attribute of jamming, (c) the area attribute of target, and (d) the area attribute of jamming in different scenarios.

$$\hat{\sigma}_k^2 = \frac{1}{N}\sum_{i=1}^{N}(x_{k,i} - \hat{\mu}_k)^2 \tag{11}$$

Therefore, the posterior probability of target class Y_i can be obtained through computing a product of posterior probabilities for variables X_k according to the following formula:

$$P(\mathbf{X} = \mathbf{x}|Y_i) = \prod_{k=1}^{n} \mathbf{N}(X_k|\hat{\mu}_k, \hat{\sigma}_k^2) \tag{12}$$

2) GAUSSIAN MIXTURE MODEL FOR FEATURE PROBABILITY DISTRIBUTION FUNCTION

Importantly, in order to better describe the characteristics of the feature distribution, the feature histograms curve can approximately be described by the Gaussian mixture model (GMM). Therefore, we assume in this paper that all of the random variables for the selected feature are distributed as per the mixed Gaussian distribution [18]:

$$\bar{\mathbf{N}}(X_k|\boldsymbol{\mu}_\mathbf{k}, \boldsymbol{\sigma}_k^2) = \sum_{j=1}^{m} \omega_{k,j}\mathbf{N}(X_k|\mu_{k,j}, \sigma_{k,j}^2) \tag{13}$$

$$\mathbf{N}(X_k|\mu_{\mathbf{k,j}}, \sigma_{k,j}^2) = \frac{1}{\sqrt{2\pi}\sigma_{k,j}}\exp(-\frac{(X_k - \mu_{k,j})^2}{2\sigma_{k,j}^2}) \tag{14}$$

where $\omega_{Y_i,j}$ is the weight coefficient of item in the mixed Gaussian distribution, and $\mu_{k,j}$, $\sigma_{k,j}^2$ are respectively the mean values and variance parameters of item m. The distribution concerns X_k feature variables. Assuming that $(X_{k1}, X_{k2}, \ldots, X_{kN})$ is an instance of X_k, its value is $(x_{k1}, x_{k2}, \ldots, x_{kN})$, $\boldsymbol{\Theta}_k = (\boldsymbol{\omega}_k, \boldsymbol{\mu}_k, \boldsymbol{\sigma}_k^2)$. The maximum likelihood (ML) [17] is taken from the training dataset $\mathbf{D}$ to estimate $\boldsymbol{\Theta}_k$. The likelihood function is represented as:

$$\mathbf{L}(\boldsymbol{\Theta}_k) = \prod_{i=1}^{N} \bar{\mathbf{N}}(x_{k,i}|\boldsymbol{\omega}_k, \boldsymbol{\mu}_k, \boldsymbol{\sigma}_k^2) \tag{15}$$

$$\mathbf{lnL}(\boldsymbol{\Theta}_k) = \sum_{i=1}^{N} \mathbf{ln}\{\sum_{j=1}^{m} \omega_{k,j}\mathbf{N}(x_{k,i}|\mu_{k,j}, \sigma_{k,j}^2)\} \tag{16}$$

Unfortunately, this represents a nonlinear function of the parameter $\boldsymbol{\Theta}_k$; therefore, direct maximization is impossible. Nevertheless, ML parameter estimation can be solved iteratively using the EM [18] approach. The iterative formula for the EM approach is as follows.

The sample data $\bar{x}_{k,i}$ are posterior probability generated by the j^{th} Gaussian distribution:

$$P(j|x_{k,i}, \boldsymbol{\Theta}_k) = \frac{\omega_j\mathbf{N}(x_{k,i}|\mu_j, \sigma_j^2)}{\sum_{i=1}^{m} \omega_t\mathbf{N}(x_{k,i}|\mu_t, \sigma_t^2)} \tag{17}$$

Furthermore, the parameter estimation of $\boldsymbol{\Theta}_k$ is as follows:

$$\hat{\omega}_j = \frac{1}{N}\sum_{i=1}^{N} P(j|x_{k,i}, \boldsymbol{\Theta}_k) \tag{18}$$

$$\hat{\mu}_j = \frac{\sum_{i=1}^{N} P(j|x_{k,i}, \boldsymbol{\Theta}_k)x_{k,i}}{\sum_{i=1}^{N} P(j|x_{k,i}, \boldsymbol{\Theta}_k)} \tag{19}$$

$$\hat{\sigma}_j^2 = \frac{\sum_{i=1}^{N} P(j|x_{k,i}, \boldsymbol{\Theta}_k)x_{k,i}^2}{\sum_{i=1}^{N} P(j|x_{k,i}, \boldsymbol{\Theta}_k)} - \hat{\mu}_j^2 \tag{20}$$

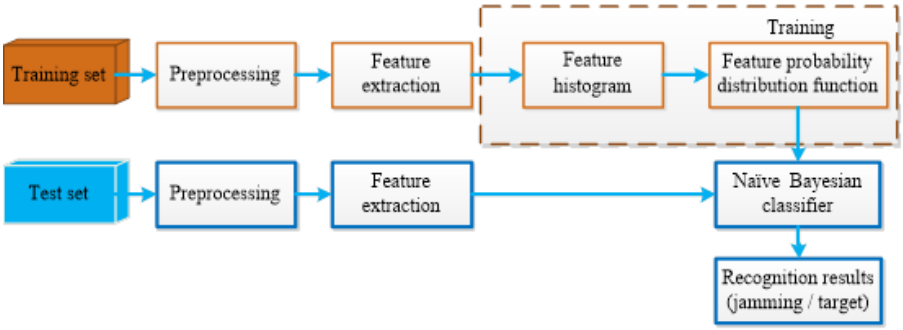

FIGURE 4. The algorithm flow chart.

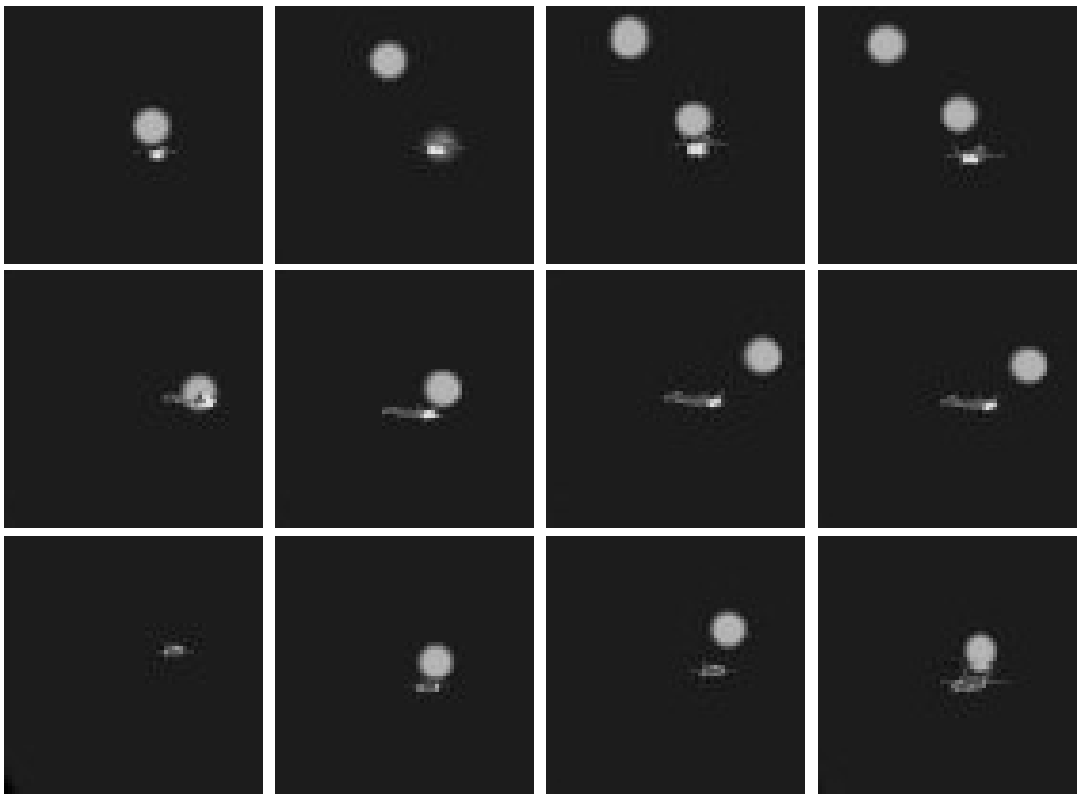

FIGURE 5. Images representing the training set generated for this paper.

Therefore, the posterior probability of target class Y_i can be obtained through computing a product of posterior probabilities for variables X_k according to the following formula:

$$P(\mathbf{X} = \mathbf{x}|Y_i) = \prod_{k=1}^{n} \bar{\mathbf{N}}(X_k|\hat{\mu}_k, \hat{\sigma}_k^2) \tag{21}$$

IV. PROPOSED APPROACH

Fig. 4 is a flow chart that illustrates the process followed by our algorithm. It is divided into 4 steps: In step 1 we generate the training and testing sets, and classify all of the instances accordingly. The second step is feature extraction from the training samples, followed by smoothing of the features and then computing the feature histogram based on Formula (7). In the third step, assuming the mixed Gaussian distribution for the feature histogram, we estimate the model's parameters based on Formulas (18) - (20) and the training data. From this we determine the feature probability distribution model. In the final step, we build a target and jamming recognition algorithm based on the naive Bayesian classifier.

A. TRAINING DATASET

Obtaining training data for this problem is a difficult task, as image data for genuine missile flights is rare. Whether in test or real life, air-combat countermeasure images are only

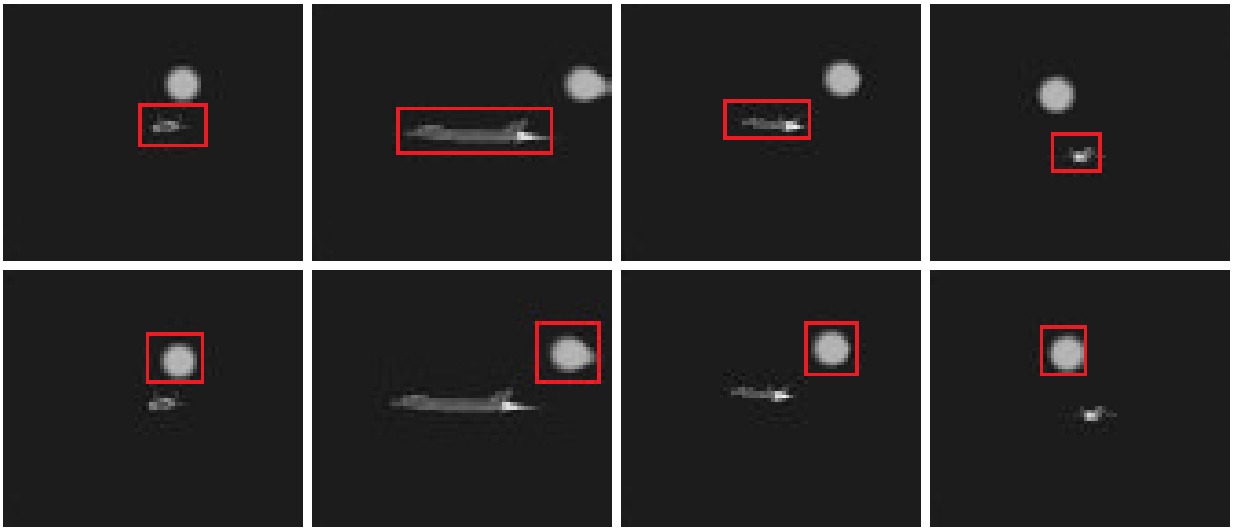

FIGURE 6. Marking of target and jamming samples in training set.

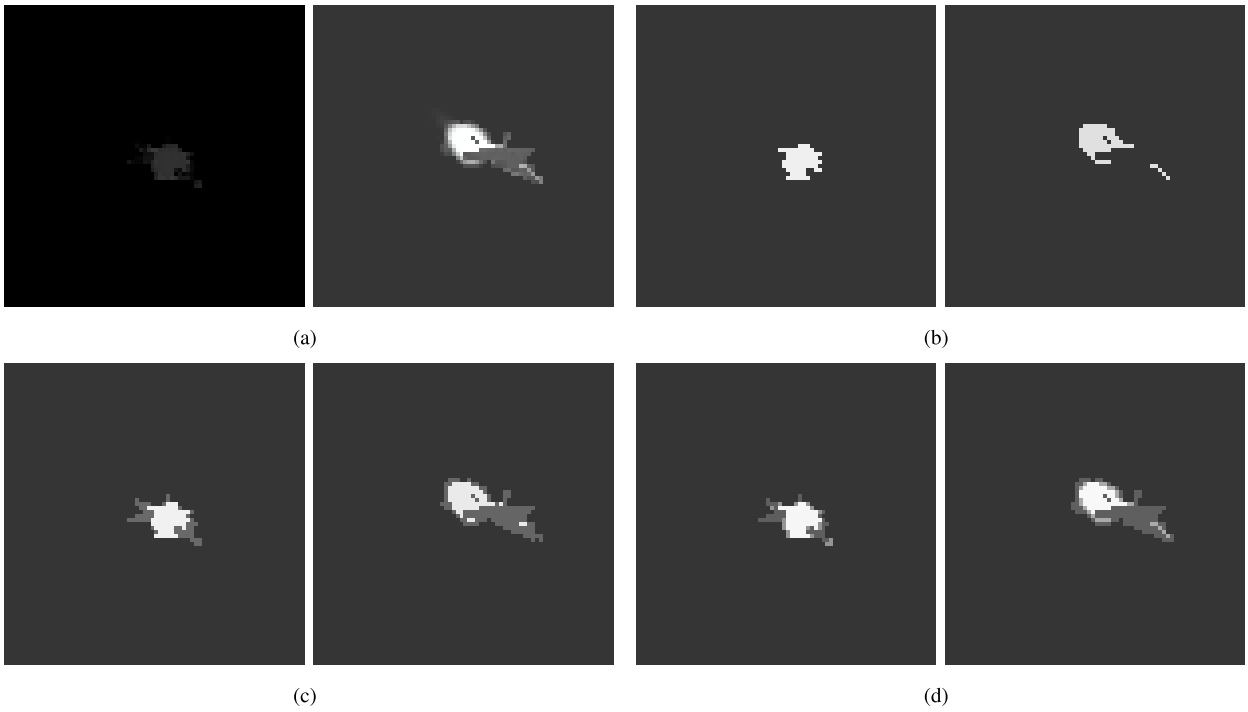

FIGURE 7. Effects of clustering the original image with 2, 3, and 4 clusters. (a) Original. (b) 2 clusters. (c) 3 clusters. (d) 4 clusters.

released to study for government bodies. This paper uses the air-combat countermeasure sample library to reproduce situations involving combat aircraft and missiles. We generate various ballistic samples through the use of advanced IR modeling and simulation techniques, and in turn, we build both a training and testing set that is used by the classifier. In order to test the target recognition performance under various jamming conditions, we use the simulation images shown in Fig.5. The images are 16-bit gray scale and the resolution is 128 $\times$ 128 pixels. The initial launching distance for jamming is 5000m 3000m, 2000m, and 1000m. There are 12,24,48 decoys launched, and the missile interval is 0.5s. There is a ballistic curve with the entrance angle (angle between the missile body and target aircraft shaft upon launching the missile) of 15° as an interval from 0° to 360°. As a whole, the following image sequence is generated.

Next, the K-means algorithm [19], [20] is used to divide the data that represents the images. The result is a separation of areas between target and jamming. The discrimination is made using the feature similarity matching approach based on the characteristics in prior knowledge. The target and jamming areas are automatically marked with the appropriate label. If there are any images that are marked incorrectly then they are relabeled accordingly (i.e. marked manually). Examples of this are shown in Fig. 6. From here, feature extraction is performed and from this we create positive and negative training samples for the target and jamming objects, with all of the selected features: $\boldsymbol{D}_+ = \{\mathbf{x}_1, \mathbf{x}_2, \ldots, \mathbf{x}_n\}$ and $\boldsymbol{D}_- = \{\mathbf{x}_1, \mathbf{x}_2, \ldots, \mathbf{x}_n\}$, $\mathbf{x}_k = \{x_{k,1}, x_{k,2}, \ldots, x_{k,N}\}$, where n is the number of features, and N is the number of samples.

B. PREPROCESSING

1) TARGET SEGMENTATION

In order to achieve the highest classification accuracy, it is important to extract the image details such that we retain the relevant information. Consequently, the images need to be preprocessed by various means including filtering, segmentation, etc. In terms of an IR image with artificial jamming present, the radiation characteristics of the IR decoy are relatively apparent. It presents as a highly bright area, similar to the areas containing the tail flow, tail flame and the head of the target aircraft. These intensely lit areas are sharply different; therefore, image segmentation based on the gray threshold makes it hard to achieve the ideal effect. For this research, we conduct image segmentation using the K-means clustering algorithm. Clusters are formed based on pixels with a similar IR gray-value. Each pixel is assigned a class based on a set of rules, and this continues until the entire image has been segmented.

The choice of the number of clusters greatly affects the generation of candidate areas, and thus the final results. If there are too few clusters, then the target body is easy to merged with the background. So, it can results in the target being split. When the number of clusters is sufficiently large then the body of the aircraft is properly represented within the extraction. As such, it is possible to discern a relatively complete target. This paper experiments with cluster sizes of 2, 3 and 4; the initial clustering centers are evenly distributed within the images. The results of our clustering are shown in Fig. 7. Based on what we learned during this test, we made the choice for the number of clusters to be 3 in the remaining experiments.

2) SELECTION AND EXTRACTION OF FEATURES

The process of selecting and extracting features involves searching for recognizable objects, or pieces, in each segment that was created. It is the responsibility of the classification algorithm to examine the available features and in turn, classify the represented objects. There are numerous prospective features present in both target and jamming scenarios, and in order to improve both speed and accuracy of classification it is important to narrow the scope. In this paper we chose to focus on features that represent the target and jamming characteristics at various imaging stages. We use the following selection criteria:

a) The selected feature should have the highest similarity with the correct target, specified by the corresponding feature in the target template;

b) The selected feature should have the lowest similarity or alternatively the highest dissimilarity with the non-like targets;

c) When the target meets a set of specific characteristics (i.e. mean gray value, area, length-width ratio, motion speed, etc.) then the target best matching these features should be selected.

Generally, the method and steps for selecting features according to the above principles are as follows:

a) Target characteristic analysis. According to the research results of the target imaging characteristics of the seeker tracking process from the far distance to near distance, the target characteristics include the point target with no shape

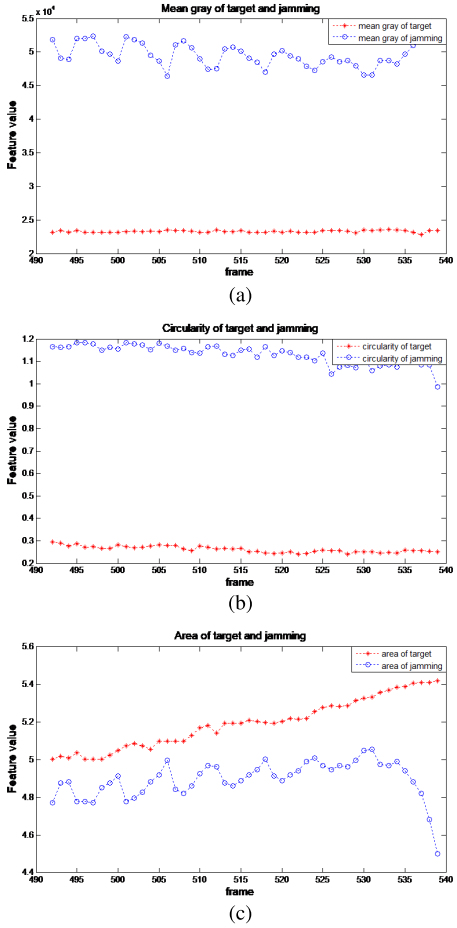

FIGURE 8. The feature variability curve of (a) the Mean Gray attribute of target, (b) the Circularity attribute, and (c) the area attribute of target and jamming in part of image data sequences.

TABLE 1. Features used in this paper.

Feature name	Feature variable	Computational formula	Description
Coordinates		(x, y)	Image pixel coordinates
Gray value		$f(x, y)$	Gray value for the pixel at (x, y) in the primitive image
Mean gray	X_1	$G_{Ave} = \frac{1}{T}\sum_1^T (f(x, y) - G_{Bkg})$	Accumulation and averaging of the differences between gray value $f(x, y)$ of pixels and the background gray in the primitive image target area
Maximum gray	X_2	$G_{Max} = f_{\max}(x, y) - G_{Bkg}$	Difference between the gray value $f_{max}(x, y)$ for the point of most intense gray as compared to the background gray in the primitive image target area
Energy	X_3	$E = \sum_1^T (f(x, y) - G_{Bkg})$	Accumulation of the differences between gray value $f(x, y)$ of T pixels and the background gray G_{Bkg} in the primitive image target area
Length-width ratio	X_4	$R = L/W$	Ratio of horizontal length L to vertical width W of the minimum exterior rectangle
Circumference	X_5	$P = \mathbf{log}_2(2 \times (W_o - 1))$	The sum of the number of pixels included in the binary image target boundary, where W_o is the width of the exterior rectangle, or the number of lines occupied by the target area
Area	X_6	$A = \mathbf{log}_2 \sum_1^W l_i$	The logarithm of the sum of the number of pixels included in the binary image target boundary, where l_i represents the cumulative sum of $f(x, y) > G_{Bkg}$ pixels in all W_o lines
Circularity	X_7	$C = P^2/A$	Ratio of the square of the circumference to the area
Complexity	X_8	$D = P/A$	Ratio of circumference to area
Rectangularity	X_9	$C = A/(L \times W)$	Ratio of target's area to the area of the minimum exterior rectangle

information, the surface target with rough outline and gray distribution, the surface target with contour structure details and gray scale distribution. Based the known and prior information, a candidate feature set is constructed;

b) Target data analysis. Based on the test and simulation dataset, the relationship between the candidate target and the jamming characteristics over time are studied. And the selected feature with obvious difference of the target and the jamming are given by analyzing the ratio between total average difference and total average target feature, which is greater than a certain threshold T;

c) Time performance test. The calculation efficiency of features are analyzed and the features are kept whose the calculation time are ms level. Finally, considering time performance and recognition performance, the available feature set is obtained.

As shown in Fig. 8, there is a large difference in the average gray level and circularity of the target and the jamming from the analysis of a selected data segment. And the calculation efficiency of these features is high. Hence, the features can be used to distinguish the target and the jamming.

Although there are many features to use and some complicated features may have better recognition performance, the time of air-to-air missile attack is very short and the image frequency of a hot imaging system is not less than 50 frames per second. Considering the tradeoff between the feature computation efficiency and recognition effect, we have selected 9 features by analyzing the feature variability and the elapsed time based on the simulation database in the jamming environment, in order to test our proposed Bayesian method for this research, as shown in Table 1.

3) FEATURE HISTOGRAM SMOOTHING

The feature histograms created during the process have obvious and significant fluctuations. This is a result of applying the generative model, as well as characteristics related to the training set. Therefore, it is beneficial to use a smoothing operation. We have done so based on the sliding window and mean value filtering approach:

$$\bar{P}(r_{k,t}) = \frac{1}{T}\sum_{t=1}^{T} P(r_{k,t}) \tag{22}$$

where T is the width of sliding window. The feature histograms, previously shown in Fig. 3, are transformed after smoothing into what is shown in Fig. 9.

C. PARAMETER SPECIFICATION OF FEATURE PROBABILITY DISTRIBUTION FUNCTION

The steps for specifying parameters for the feature probability distribution function is shown in Algorithm 1.

The feature probability distribution function expression using Gauss model(GM) for mean gray and the area of target in Table 1 is as follows:

$$\bar{\mathbf{N}}_t(X_1|\mu_1, \sigma_1^2) = a_1 \cdot \frac{1}{\sqrt{2\pi}\sigma_1} e^{-\frac{(x-\mu_1)^2}{2\sigma_1^2}} = 0.1202 \cdot e^{-(\frac{x-21350}{1742})^2} \tag{23}$$

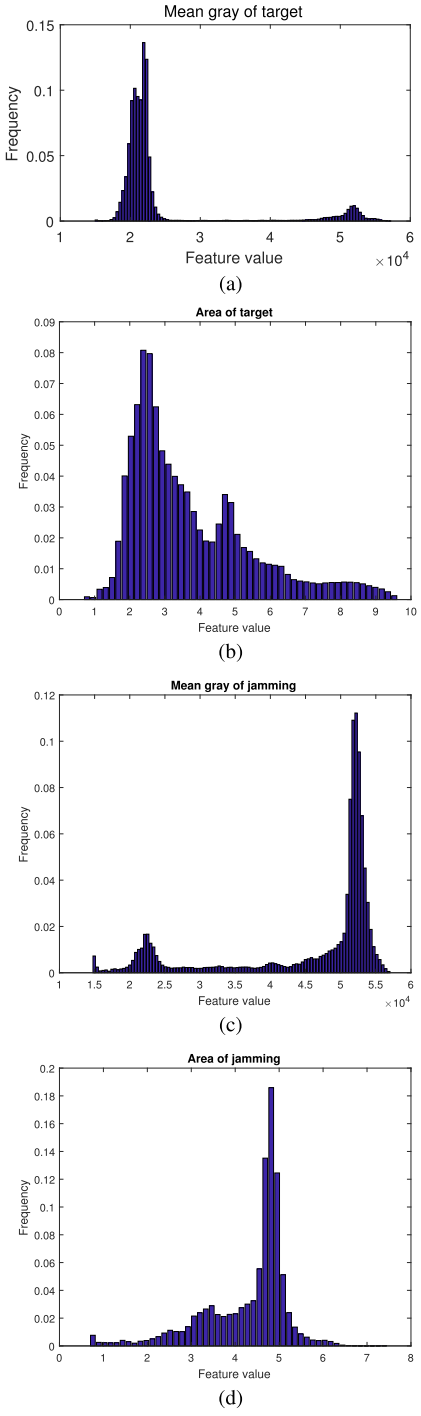

FIGURE 9. Feature histogram of (a) the mean gray attribute of target, (b) the mean gray attribute of jamming, (c) the area attribute of target, and (d) the area attribute of jamming post smoothing in different scenarios.

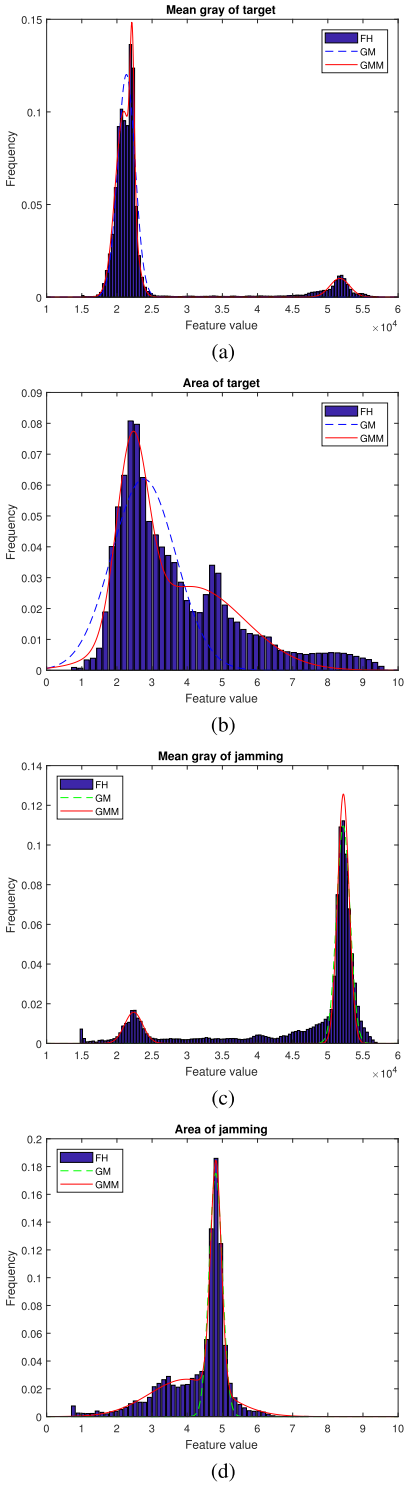

FIGURE 10. Curve comparison between the GM feature probability distribution function, GMM feature probability distribution function, and feature histogram of: (a) the mean gray attribute of target, (b) the mean gray attribute of jamming, (c) the area attribute of target, and (d) the area attribute of jamming.

$$\bar{\mathbf{N}}_t(X_6|\mu_6,\sigma_6^2) = a_1 \cdot \frac{1}{\sqrt{2\pi}\sigma_1} e^{-\frac{(x-\mu_1)^2}{2\sigma_1^2}} = 0.0620 \cdot e^{-(\frac{x-2.761}{1.289})^2} \quad (24)$$

The feature probability distribution function expression using GM for the mean gray and area of jamming is as follows:

$$\bar{\mathbf{N}}_t(X_1|\mu_1,\sigma_1^2) = a_1 \cdot \frac{1}{\sqrt{2\pi}\sigma_1} e^{-\frac{(x-\mu_1)^2}{2\sigma_1^2}} = 0.1096 \cdot e^{-(\frac{x-52200}{1363})^2} \quad (25)$$

Algorithm 1 Parameter Specification for the Feature Probability Distribution Function.

1: Construct the training set $\mathbf{D}$, then acquire exterior rectangle areas related to both target and jamming objects. This is done based on the automatic and artificial marking approaches. Compute $X_1, X_2, X_3, \ldots, X_n$ for all n selected feature variables and build training sets for the target and jamming scenarios: $\mathbf{D}_+ = \{\mathbf{x}_1, \mathbf{x}_2, \ldots, \mathbf{x}_n\}$ and $\mathbf{D}_- = \{\mathbf{x}_1, \mathbf{x}_2, \ldots, \mathbf{x}_n\}$, $\mathbf{x}_k = \{x_{k,1}, x_{k,2}, \ldots, x_{k,N}\}$, where $k = 1, 2, \ldots, n$;
2: Compute histograms for all features using Formulas (8) and (22). Perform the smoothing and then conduct a statistical analysis of the wave crest over the histograms for $X_1, X_2, X_3, \ldots, X_n$. Determine the Gaussian mixture model items m;
3: Determine the Gaussian mixture distribution model parameters $\theta_k = (\mu_k, \sigma_k)$ as (10) and (11). And determine the Gaussian mixture distribution model parameters $\theta_k = (\omega_k, \mu_k, \sigma_k)$ as (18)-(20).

$$\bar{\mathbf{N}}_t(X_6|\mu_6, \sigma_6^2) = a_1 \cdot \frac{1}{\sqrt{2\pi}\sigma_1} e^{-\frac{(x-\mu_1)^2}{2\sigma_1^2}} = 0.1752 \cdot e^{-(\frac{x-4.81}{0.265})^2} \quad (26)$$

The feature probability distribution function expression using Gauss mixed model (GMM) for mean gray and the area of target in Table 1 is as follows:

$$\begin{aligned}\bar{\mathbf{N}}_t(X_1|\mu_1, \sigma_1^2) = a_1 \cdot \frac{1}{\sqrt{2\pi}\sigma_1} e^{-\frac{(x-\mu_1)^2}{2\sigma_1^2}} \\ + a_2 \cdot \frac{1}{\sqrt{2\pi}\sigma_2} e^{-\frac{(x-\mu_2)^2}{2\sigma_2^2}} \\ + a_2 \cdot \frac{1}{\sqrt{2\pi}\sigma_3} e^{-\frac{(x-\mu_3)^2}{2\sigma_3^2}} \\ = 0.08453 \cdot e^{-(\frac{x-22170}{417.3})^2} \\ + 0.1003 \cdot e^{-(\frac{x-20990}{1722})^2} \\ + 0.0101 \cdot e^{-(\frac{x-51700}{1979})^2} \quad (27)\end{aligned}$$

$$\begin{aligned}\bar{\mathbf{N}}_t(X_6|\mu_6, \sigma_6^2) = a_1 \cdot \frac{1}{\sqrt{2\pi}\sigma_1} e^{-\frac{(x-\mu_1)^2}{2\sigma_1^2}} \\ + a_2 \cdot \frac{1}{\sqrt{2\pi}\sigma_2} e^{-\frac{(x-\mu_2)^2}{2\sigma_2^2}} \\ = 0.0627 \cdot e^{-(\frac{x-2.4380}{0.6338})^2} \\ + 0.02708 \cdot e^{-(\frac{x-4.1190}{2.134})^2} \quad (28)\end{aligned}$$

The feature probability distribution function expression using GMM for the mean gray and area of jamming is as follows:

$$\begin{aligned}\bar{\mathbf{N}}_t(X_1|\mu_1, \sigma_1^2) \\ = a_1 \cdot \frac{1}{\sqrt{2\pi}\sigma_1} e^{-\frac{(x-\mu_1)^2}{2\sigma_1^2}} + a_2 \cdot \frac{1}{\sqrt{2\pi}\sigma_2} e^{-\frac{(x-\mu_2)^2}{2\sigma_2^2}} \\ = 0.1257 \cdot e^{-(\frac{x-52210}{1149})^2} + 0.01574 \cdot e^{-(\frac{x-22380}{1814})^2} \quad (29)\end{aligned}$$

$$\begin{aligned}\bar{\mathbf{N}}_t(X_6|\mu_6, \sigma_6^2) \\ = a_1 \cdot \frac{1}{\sqrt{2\pi}\sigma_1} e^{-\frac{(x-\mu_1)^2}{2\sigma_1^2}} + a_2 \cdot \frac{1}{\sqrt{2\pi}\sigma_2} e^{-\frac{(x-\mu_2)^2}{2\sigma_2^2}} \\ = 0.1646 \cdot e^{-(\frac{x-4.817}{0.2157})^2} + 0.0296 \cdot e^{-(\frac{x-3.988}{1.511})^2} \quad (30)\end{aligned}$$

As shown in Fig. 10, solving the feature probability distribution function through Gauss model and Gauss mixed model based on the training dataset can result in a change of the feature histogram (FH). This can then be used as prior knowledge for the naive Bayesian classifier.

Algorithm 2 Proposed Recognition Algorithm

1: The K-means segmentation algorithm explores and processes the image area. The resulting segments contain the acquired image primitive data in the connected areas. With the background set to 0, each area is considered as an input feature vector to be classified;
2: The feature vector $\mathbf{X} = (X_1, X_2, X_3, \ldots, X_9)$ represents the feature variable, as shown in Table 1, where $\mathbf{x} = (x_1, x_2, x_3, \ldots, x_9)$ represents the 9 feature values in the area to be classified. This will take place for each test image $\mathbf{I}$ in the test set;
3: Define category set $\mathbf{Y}_C = \{Y_1, Y_2\}$, where Y_1represents the target aircraft, and Y_2 represents jamming efforts;
4: Compute the posterior probabilities $P(\mathbf{X} = \mathbf{x}|Y_1)$, $P(\mathbf{X} = \mathbf{x}|Y_2)$ of the classes Y_1, Y_2, based on Formula (12) and (21). This is calculated using the probability distribution function of the 9 features based on Formulas (23) - (30);
5: Compute class prior probability based on Formula (7), and compute the posterior probability $P(Y_1|\mathbf{X} = \mathbf{x})$, $P(Y_2|\mathbf{X} = \mathbf{x})$, based on Formula (5);
6: As per the naive Bayesian classifier and the maximum posterior criterion, compute the maximum posterior probability based on Formula (6). In the recognition algorithm described, if $P(Y_1|\mathbf{x}) > P(Y_2|\mathbf{x})$, $\mathbf{x} = (\bar{x}_{k1}, \bar{x}_{k2}, \ldots, \bar{x}_{kN})^T$ belongs to the target feature template, rather than the jamming feature template, then recognition of the target is accomplished.

D. RECOGNITION ALGORITHM WITH BAYESIAN CLASSIFIER

The anti-countermeasure, aerial IR target recognition algorithm that we have founded on the naive Bayesian classifier is described in Algorithm 2.

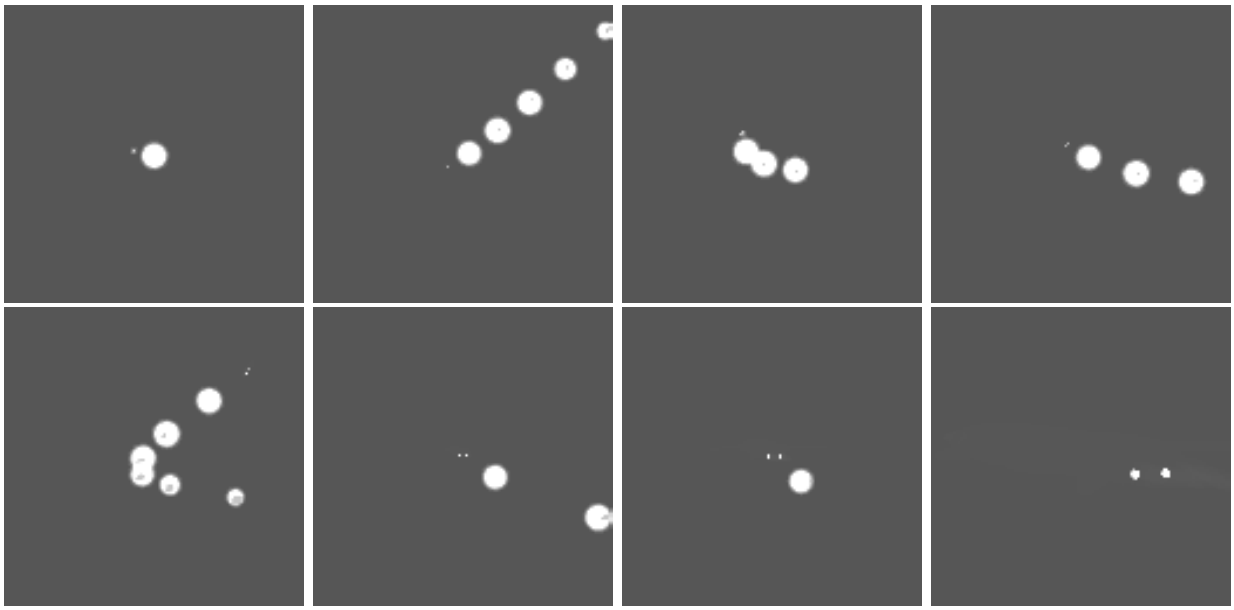

FIGURE 11. Aerial jamming environment simulation test image.

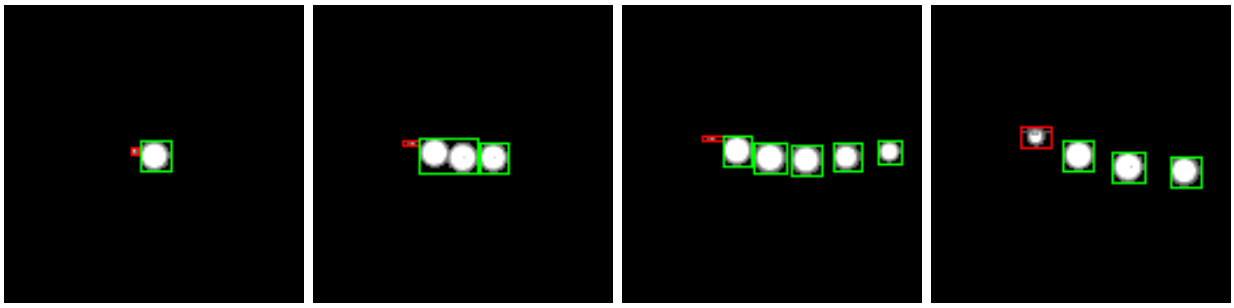

FIGURE 12. Recognition results for initial jamming launch distance of 3000 m.

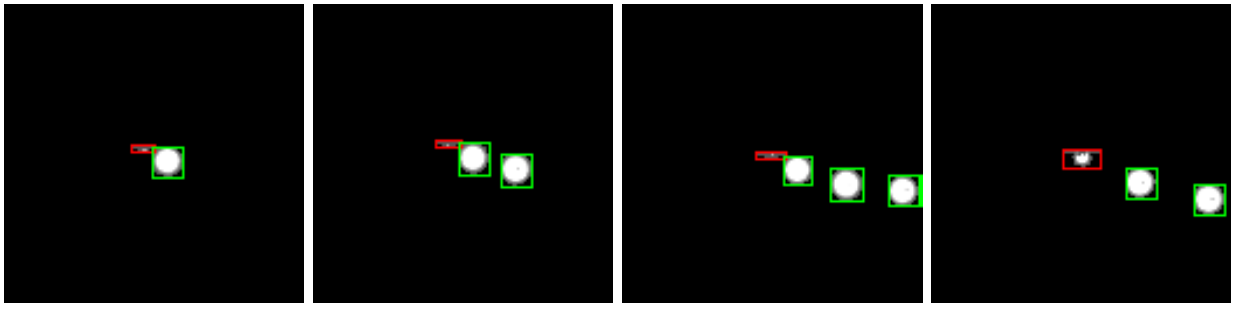

FIGURE 13. Recognition results for initial jamming launch distance of 2000 m.

V. EXPERIMENTAL RESULTS

In this section, we assess the performance of our aircraft target recognition algorithm in various jamming scenarios. The parameter settings for the simulation of the IR scenario test images is as follows: the background is simple and uniform; the number of launched IR decoys can be set to 12, 24 and 48; the interval of launched IR decoys can be set to 0.4s, 0.5s, 0.7s and 1.0s; the target altitude of both missile and aircraft is identical, and the distance is 8000m; the various angles of view at the same horizontal plane (centered by aircraft, represented by azimuth angle between missile and aircraft) are respectively 10°, 30°, 60° and 90°; the initial launching distances of the jamming efforts can be respectively set to 5000m, 3000m, 2000m and 1000m. The simulation test image is shown in Fig. 11.

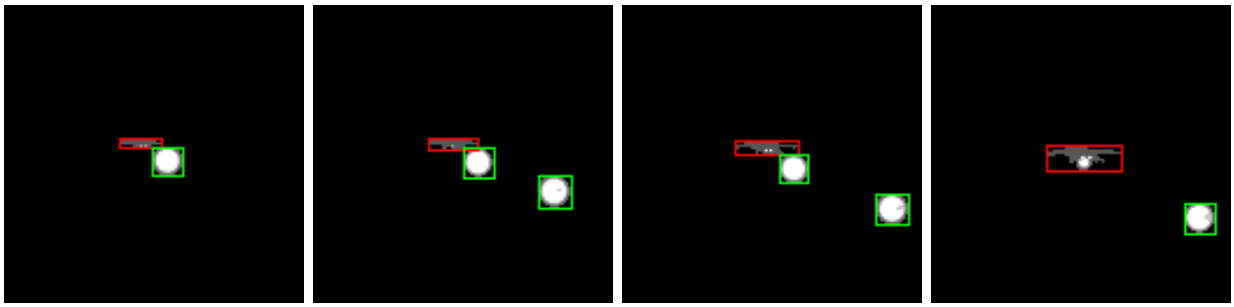

FIGURE 14. Recognition results for initial jamming launch distance of 1000 m.

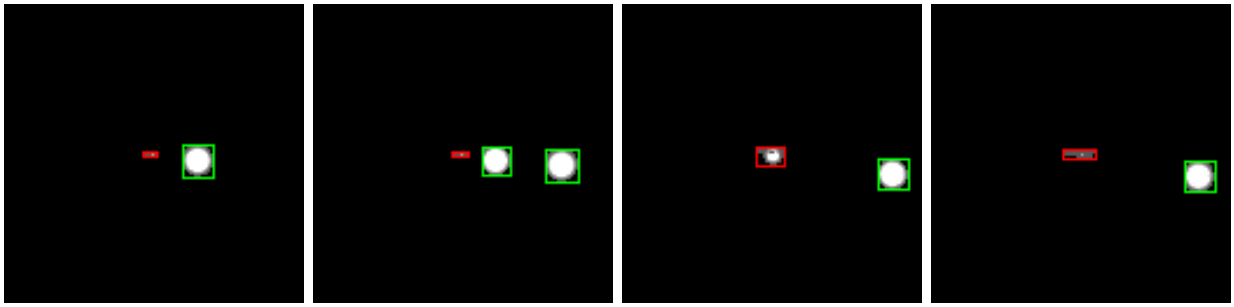

FIGURE 15. Recognition results at 30° azimuth angle.

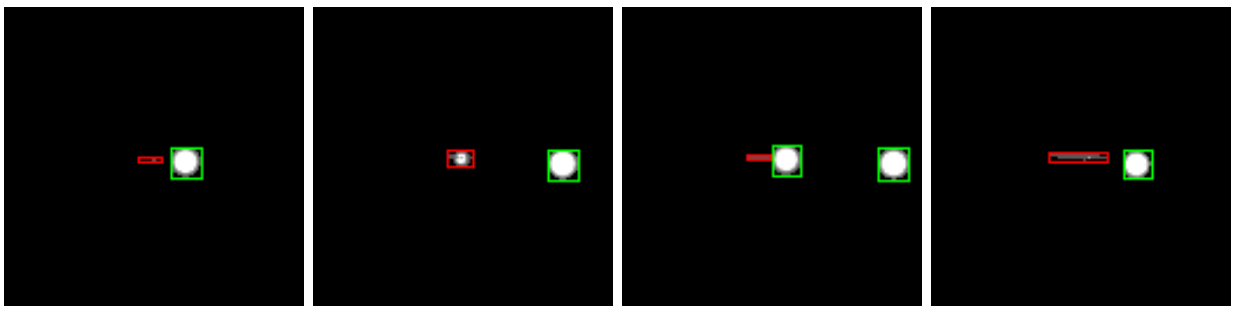

FIGURE 16. Recognition results at 60° azimuth angle.

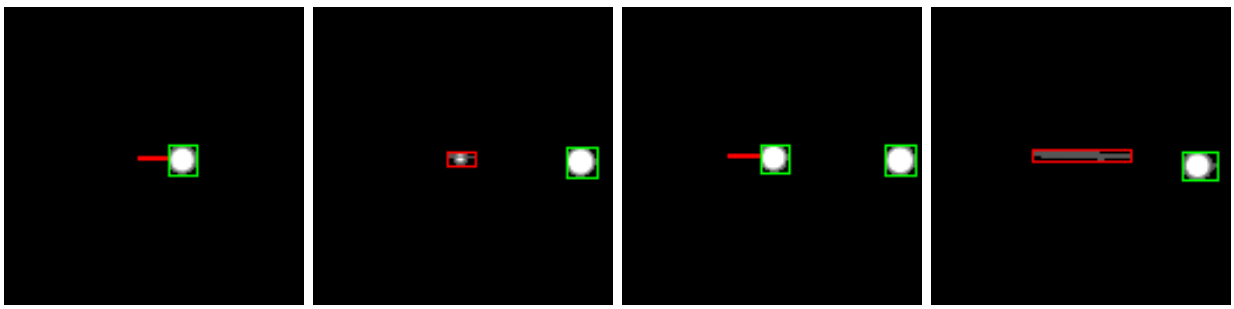

FIGURE 17. Recognition results at 90° azimuth angle.

A. ANALYSIS OF TARGET RECOGNITION RESULTS FOR JAMMING ENVIRONMENTS WITH DECOYS LAUNCHED AT VARIOUS DISTANCES

The relative azimuth angle is 10°. For initial jamming launch distances of 3000m, 2000m and 1000m, the recognition results of our algorithm using GMM feature probability distribution function are respectively shown in Fig. 12, Fig. 13 and Fig. 14. The target aircraft is marked with a red rectangular box, and the IR decoy is framed in green. The above illustrated simulation experiments have shown that the targets and

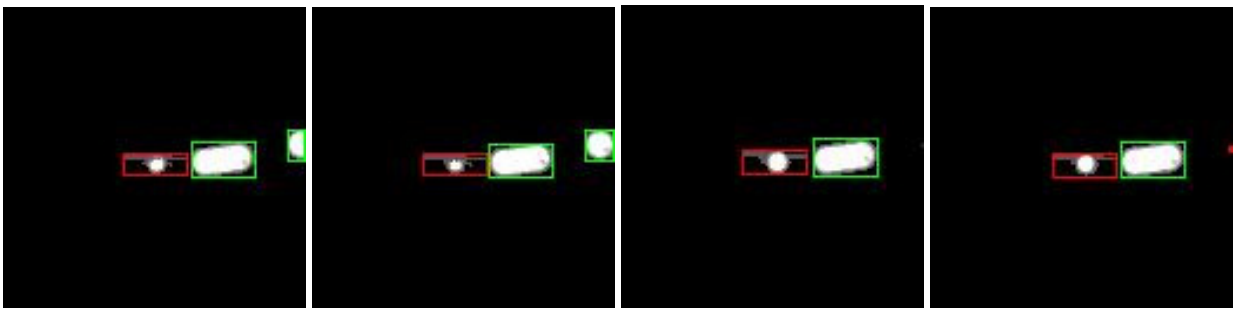

FIGURE 18. Recognition results with 2 decoys being launched once at 10° azimuth angle.

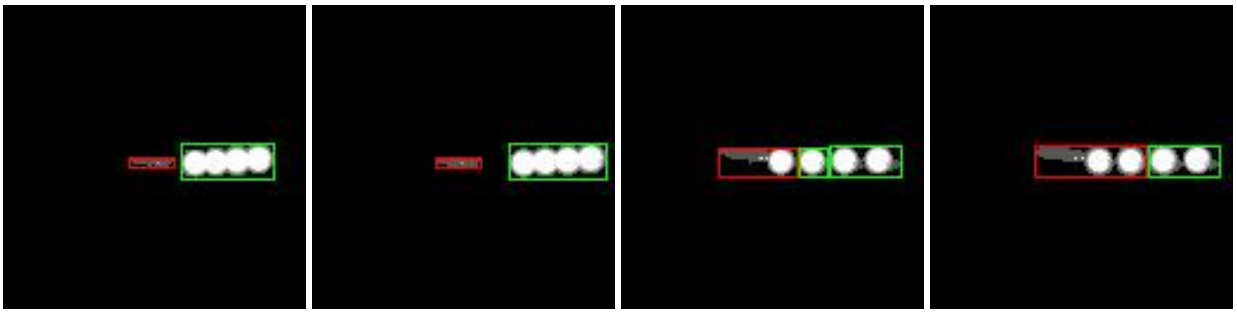

FIGURE 19. Recognition results with 4 decoys being launched once at 60° azimuth angle.

TABLE 2. Target recognition results under various situational conditions.

Distance (m)	Relative azimuth angle (°)	Launching conditions	Feature matching algorithm accuracy (%)	Our target recognition algorithm accuracy (%)	
				GM	GMM
1000	10	Number of	61.2	72	84.1
2000	10	launched	50.8	59.6	68.2
3000	10	decoys=12;	30.0	34.2	40.9
1000	30	interval of	70.1	80.5	94.4
2000	30	launched	61.9	70.9	87.3
3000	30	decoys=0.5s	59.0	64.2	69.9
1000	60		71.9	84.5	99.4
2000	60		62.8	80.9	96.4
3000	60		59.1	69.4	84.3
1000	90		73.1	82.6	99.4
2000	90		65.7	83.9	98.2
3000	90		60.2	75.9	90.3

jamming efforts have been completely separated. Regardless of whether the launch distance was short, medium or long, the features of both target and jamming are relatively significant. Testing indicates that our algorithm achieves better than 90% target recognition accuracy.

When the target and jamming objects overlap in the image, the algorithm suffers from degrading performance for both medium and long launch distances. Considering the marking of the training samples and the feature probability distribution, the target recognition accuracy for these distances is relatively low. At the same time, however, the performance at short distances does not significantly deteriorate. Post analysis has revealed that this is related to the shape and gray distribution features. These are relatively apparent at low distances, and thus the degree of feature confusion is relatively small. Hence, the classification accuracy is still relatively high.

B. ANALYSIS OF TARGET RECOGNITION RESULTS FOR JAMMING ENVIRONMENTS WITH DECOYS LAUNCHED AT DIFFERENT ANGLES OF VIEW

This next group of experiments involves launching decoys at various azimuth angles. The initial launching distance is fixed at 3000m, while the azimuth angles are 30°, 60° and 90°. The results of our algorithm using GMM are illustrated in Fig. 15, Fig. 16 and Fig. 17. The target aircraft is marked with a red rectangular box, and the IR decoy is framed in green.

The simulation experiments illustrated in Fig. 12, Fig. 15, Fig. 16 and Fig. 17 correspond to azimuth angles of 10°, 30°, 60° and 90°. At a 3000m, the launch distance for all

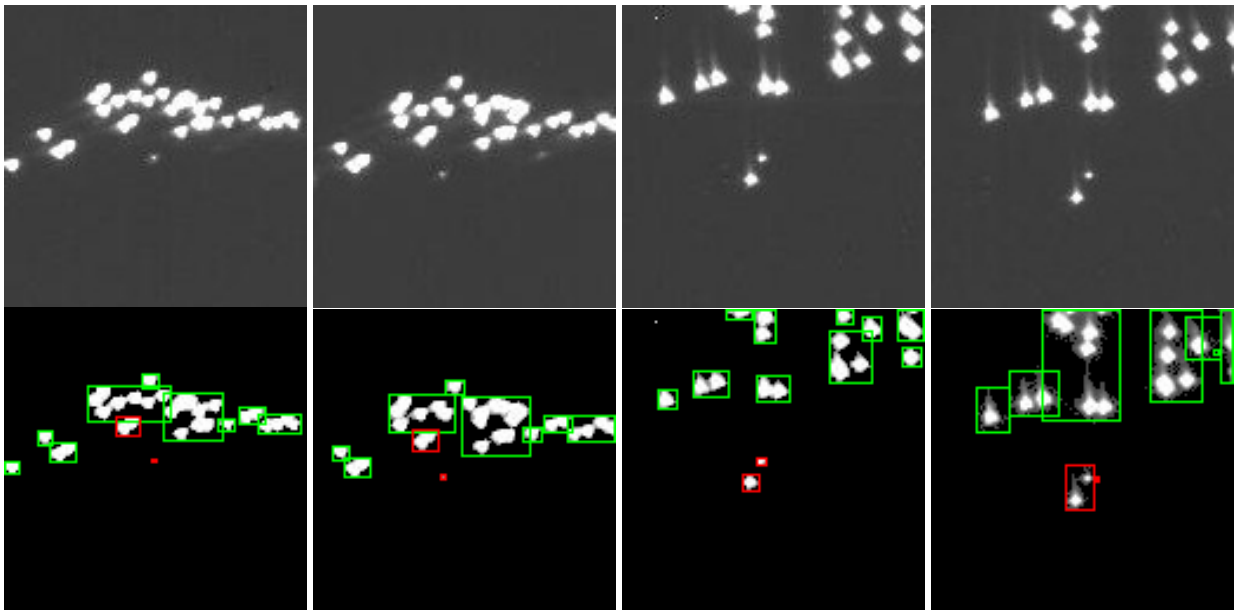

FIGURE 20. Recognition results with a large number of decoys in the real jamming environments.

is considered long. The time that the target is obscured by IR decoys is relatively small, and it follows that the degree of feature confusion is comparatively small. In this case, the accuracy of training sample marking and the feature probability distribution function is relatively high. Consequently, the target recognition accuracy also increases. As mentioned above, at short distances the shape and gray distribution features are relatively apparent. Hence, the degree of feature confusion is relatively small and the target recognition accuracy remains high. The target recognition rate can be defined as follows:

$$P_r = \frac{N_r}{N_t} \times 100\% \tag{31}$$

where N_r represents the number of images for which the recognition was successful, and N_t represents a total number of test images including both target and IR decoy. Fig.3 shows a comparison of our algorithm using GM and GMM feature probability distribution function against the feature matching algorithm based on the datasets generated for our research. It is clear that the accuracy of our algorithm surpasses that of the feature matching algorithm. And the accuracy of our algorithm using GMM feature probability distribution function is better than GM feature probability distribution function.

C. ANALYSIS OF TARGET RECOGNITION RESULTS UNDER THE DIFFERENT LAUNCHING CONDITIONS OF IR DECOYS

This following group of experiments involves launching decoys with various strategies. First, the initial launching distance is fixed at 5000m, while the azimuth angles are 10°, 30°, 60° and 90°. Second, the launching intervals can be set to 0.4s, 0.7s, and 1.0s, while the numbers of decoys to be launched once are 1, 2 and 4. And the total numbers of decoys are 12, 24 and 48. The results with 2 and 4 decoys being launched once are illustrated in Fig. 18 and Fig. 19, where the target aircraft is marked with a red rectangular box, and the IR decoy is marked with a green rectangular box.

Further, The recognition results of our algorithm using GMM are listed in Table 4. Some regular pattern can be draw. First, the recognition probability is become greater when the launching intervals are from 0.4s to 1.0s. Second, the recognition probability is become smaller when the numbers of launched decoys once are from 1 to 4 and the total numbers of launched decoys are from 12 to 48. As mentioned above, the influence of launching strategies is relatively apparent for the obscured time and the degree of feature confusion generated by IR decoys.

D. TARGET RECOGNITION TESTS IN THE REAL JAMMING ENVIRONMENTS

This final group of experiments involves target recognition in the real jamming environments. The results of our algorithm using GMM are illustrated in Fig. 19. The target aircraft is marked with a red rectangular box, and the IR decoy is framed in green. Fig. 20 shows that the real jamming environments may be complex very much. So, our algorithm using GMM feature probability distribution function has a certain effects and the average accuracy of target recognition algorithm is less than 0.3. Hence, it is close to the simulation results at the azimuth angles of 10° from table 3, in which the launching intervals are 0.4s and the total numbers of launched decoys are 48 with 4 decoys launched once.

TABLE 3. Target recognition results under various conditions of launched decoys.

The initial launching Distance(m)	Relative azimuth angle (°)	Launching conditions			Our method (%)
		The interval of launched decoys (s)	Number of launched decoys once	The total number of launched decoys	
5000	10	0.4	1	12	49.6
5000	10	0.4	2	24	43.6
5000	10	0.4	4	48	40.9
5000	10	0.7	1	12	56.5
5000	10	0.7	2	24	51.5
5000	10	0.7	4	48	43.3
5000	10	1.0	1	12	64.4
5000	10	1.0	2	24	61.5
5000	10	1.0	4	48	27.1
5000	30	0.4	1	12	76.0
5000	30	0.4	2	24	69.5
5000	30	0.4	4	48	10.1
5000	30	0.7	1	12	83.8
5000	30	0.7	2	24	76.0
5000	30	0.7	4	48	42.4
5000	30	1.0	1	12	87.9
5000	30	1.0	2	24	84.6
5000	30	1.0	4	48	59.7
5000	60	0.4	1	12	94.9
5000	60	0.4	2	24	90.5
5000	60	0.4	4	48	25.0
5000	60	0.7	1	12	96.2
5000	60	0.7	2	24	80.4
5000	60	0.7	4	48	28.9
5000	60	1.0	1	12	97.0
5000	60	1.0	2	24	93.0
5000	60	1.0	4	48	31.1
5000	90	0.4	1	12	98.0
5000	90	0.4	2	24	97.6
5000	90	0.4	4	48	51.9
5000	90	0.7	1	12	98.3
5000	90	0.7	2	24	98.5
5000	90	0.7	4	48	50.0
5000	90	1.0	1	12	99.2
5000	90	1.0	2	24	97.7
5000	90	1.0	4	48	51.3

VI. CONCLUSION AND FUTURE WORK

This paper proposes a novel target recognition algorithm that operates in an aerial combat environment where heat seeking missile countermeasures are employed. The algorithm is based on a Bayesian probabilistic model that was developed in several stages. These include generating valid training and testing sets using a simulation, and then building a feature variable probability distribution model for each set. The model has a mixed Gaussian distribution. Next, a classification algorithm was trained to solve the problem of a low target recognition rate due to jamming. Experimental results have shown that our Bayesian approach performs superiorly when compared to the feature similarity matching algorithm. These tests were performed using our generated test datasets. Future work for this research includes improving the sample datasets, modifying the model using the measured data of IR decoys, extracting additional image information to form more reasonable prior distribution under the proposed Bayesian framework, to build a more accurate feature probability distribution function, and to consider the relation of feature variable for a better Bayesian network.

REFERENCES

[1] Z. Li, X. Wang, Z. Shen, J. Lu, and X. Ni, "Mechanisms for the millisecond laser-induced functional damage to silicon charge-coupled imaging sensors," *Appl. Opt.*, vol. 54, pp. 378–388, Jan. 2015.

[2] L. Wang, N. Jiang, and M.-S. Lv, "Research into the usage of integrated jamming of ir weakening and smoke-screen resisting the ir imaging guided missiles," *Proc. SPIE*, vol. 9674, Oct. 2015, Art. no. 967421.

[3] G. J. Gray, N. Aouf, M. A. Richardson, B. Butters, and R. H. Walmsley, "Countermeasure effectiveness against an intelligent imaging infrared anti-ship missile," *Opt. Eng.*, vol. 52, no. 2, 2013, Art. no. 026401.

[4] H. Ma, Y. Hou, and G. Su, "A robust approach for anti-jamming target tracking in forward looking infrared imagery," in *Proc. 6th Int. Conf. Image Graph. (ICIG)*, Aug. 2011, pp. 636–641.

[5] T. Badal, N. Nain, and M. Ahmed, "Multi-object trajectory coupling using online target specific decision making," in *Proc. IEEE Int. Conf. Identity, Secur. Behav. Anal. (ISBA)*, Feb. 2017, pp. 1–6.

[6] S.-Z. Wang, H.-B. Nie, and C.-J. Shi, "A drifting trajectory prediction model based on object shape and stochastic motion features," *J. Hydrodynamics, Ser. B*, vol. 26, no. 6, pp. 951–959, Jan. 2015.

[7] F. Qiang and Y. Wenxian, "Automatic target recognition based on incoherent radar returns," in *Proc. IEEE Nat. Aerosp. Electron. Conf. (NAECON)*, May 1995, vol. 1, pp. 123–128.

[8] G. Marsiglia, L. Fortunato, A. Ondini, and G. Balzarotti, "Template matching techniques for automatic IR target recognition in real and simulated scenarios: Tests and evaluations," *Proc. SPIE*, vol. 5094, pp. 159–170, Sep. 2003.

[9] J. D. Tubbs, "A note on binary template matching," *Pattern Recognit.*, vol. 22, no. 4, pp. 359–365, 1989.
[10] S. Xu, "Bayesian Naïve Bayes classifiers to text classification," *J. Inf. Sci.*, vol. 44, no. 1, pp. 48–59, 2018.
[11] G. Feng, S. Li, T. Sun, and B. Zhang, "A probabilistic model derived term weighting scheme for text classification," *Pattern Recognit. Lett.*, vol. 110, pp. 23–29, Jul. 2018.
[12] X. Zhang, C. Zhu, S. Wang, Y. Liu, and M. Ye, "A Bayesian approach to camouflaged moving object detection," *IEEE Trans. Circuits Syst. Video Technol.*, vol. 27, no. 9, pp. 2001–2013, Sep. 2017.
[13] D. C. Knill, D. Kersten, and A. Yuille, *Perception as Bayesian Inference*. D. C. Knill and W. Richards, Eds. Cambridge, U.K.: Cambridge Univ. Press, 1996, pp. 1–21.
[14] M. A. Goodale and A. D. Milner, "Separate visual pathways for perception and action," *Trends Neurosci.*, vol. 15, no. 1, pp. 20–25, 1992.
[15] T. S. Lee, "Top-down influence in early visual processing: A Bayesian perspective," *Physiol. Behavior*, vol. 77, nos. 4–5, pp. 645–650, 2002.
[16] J. Yuan, Z. Wang, Y. Sun, W. Zhang, and J. Jiang, "An effective pattern-based Bayesian classifier for evolving data stream," *Neurocomputing*, vol. 295, pp. 17–28, Jun. 2018.
[17] W. Zhang, Z. Zhang, H.-C. Chao, and F.-H. Tseng, "Kernel mixture model for probability density estimation in bayesian classifiers," *Data Mining Knowl. Discovery*, vol. 32, no. 3, pp. 675–707, May 2018.
[18] D. Reynolds, *Gaussian Mixture Models*, 2009.
[19] N. Dhanachandra, K. Manglem, and Y. J. Chanu, "Image segmentation using k-means clustering algorithm and subtractive clustering algorithm," *Procedia Comput. Sci.*, vol. 54, pp. 764–771, 2015.
[20] J. A. Hartigan and M. A. Wong, "Algorithm AS 136: A k-means clustering algorithm," *Appl. Statist.*, vol. 28, no. 1, pp. 100–108, 1979.

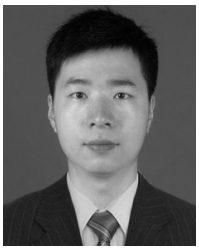

SHAOYI LI received the bachelor's degree in measurement and control technology from Southwest Jiaotong University, Chengdu, China, in 2008, and the master's and Ph.D. degrees in navigation, guidance, and control from Northwestern Polytechnical University, Xi'an, China, in 2011 and 2015, respectively, where he is currently an Assistant Researcher with the School of Aerospace. He has authored or coauthored over 10 papers in scientific journals and conference proceedings. His current research interests include ATR based on infrared image, artificial intelligence, and image processing.

KAI ZHANG received the bachelor's, master's, and Ph.D. degrees in navigation, guidance, and control from Northwestern Polytechnical University, Xi'an, China, in 2001, 2004, and 2009, respectively. He is currently an Associate Professor with the School of Aerospace, Northwestern Polytechnical University, Xi'an, China. He has authored or coauthored over 20 papers in scientific journals and conference proceedings. His current research interests include infrared imaging, artificial intelligence, and infrared scene modeling and simulation.

JIANFEI YIN received the bachelor's degree in detection, guidance, and control from Northwestern Polytechnical University, Xi'an, China, in 2001. He is currently a Researcher with the Shanghai Aerospace Control Technology Institute, Shanghai, China. He has completed many projects about hot imaging seeker and image processing. He has authored or coauthored five papers in scientific journals and conference proceedings. His current research interests include hot imaging seeker, ATR based on infrared image, and image processing.

KAI YANG received the bachelor's degree in communication engineering from Chang'an University, Xi'an, China, in 2016. She is currently pursuing the master's degree with the School of Aerospace, Northwestern Polytechnical University, Xi'an. She has authored or coauthored two papers in scientific journals and conference proceedings. Her current research interests include ATR based on infrared image and pattern recognition.